The Egyptian Journal of Neurology, Psychiatry and Neurosurgery

RESEARCH

Open Access

Dynamic channelwise functional-connectivity states extracted from resting-state EEG signals of patients with Parkinson's disease

Hao Ding[1], Xinmeng Weng[1], Minghuan Xu[1], Jian Shen[2] and Zhanxiong Wu[1*]

Abstract

Background Parkinson's disease (PD) is a progressive neurodegenerative disease that usually happens to elderly people, with a wide range of motor and dementia symptoms. An objective and convenient biomarker for PD detection is extremely valuable, especially one that could be acquired non-invasively and low-costly. To this end, this study used resting-state scalp electroencephalography (EEG) signals to explore dynamic functional-connectivity (dFC) states between each pair of EEG recording channels, without source localization.

Methods dFC refers to synchronization patterns over time between each pair of EEG channels. First, five frequency bands were extracted from EEG signals with fourth-order Butterworth bandpass filter, including delta (0.5–4 Hz), theta (4–8 Hz), alpha (8–13 Hz), beta (8–30 Hz) and gamma (30–50 Hz). Then, after non-random joint fluctuation was measured with weighted symbolic mutual information (wSMI) algorithm, whole-brain dynamic channelwise dFC states were estimated, and classified with *k*-means clustering. At last, FC state occurrences were calculated, and ANOVA analyses were performed for each state. Two open-source resting-state EEG data sets (https://doi.org/10.18112/openneuro.ds002778.v1.0.4: 32 channels, 16 health controls and 15 PD subjects. https://doi.org/10.18112/openneuro.ds003490.v1.1.0: 64 channels, 25 health controls and 25 PD subjects) were used to test our methods.

Results Significant changes in proportions of various dFC states within beta frequency-band were consistently observed in these both data sets (p value < 0.05).

Conclusions Our findings suggest that channelwise dFC states within beta frequency-band directly extracted from resting-state scalp–EEG recordings could potentially serve as a biomarker of PD.

Keywords Parkinson's disease (PD), Resting state, Electroencephalogram (EEG), Weighted symbolic mutual information (wSMI), *k*-means clustering

Background

Following Alzheimer's disease (AD), Parkinson's disease (PD) is the second most common neurodegenerative disease in elderly subjects, with the symptoms of akinesia, bradykinesia, rigidity, tremor, postural, balance instability, and other none-motor symptoms [1, 2]. It could severely affect the patients' daily life. Accurate diagnosis of PD is always difficult because of the complex etiology and the variety of clinical symptoms, especially in the

*Correspondence:
Zhanxiong Wu
wzx@hdu.edu.cn
[1] School of Electronic Information, Hangzhou Dianzi University, Hangzhou 310018, Zhejiang, China
[2] Neurosurgery Department, The First Affiliated Hospital of Zhejiang University School of Medicine, Zhejiang University, Hangzhou, China

early stage of the disease. As cognition impairment precedes motor symptoms and worsen as the disease progresses [3, 4], there has been a lot of interest in finding trustworthy biomarkers for early diagnosis of PD. For this purpose, as electroencephalogram (EEG) provides a simple, portable, non-invasive, and low-cost alternative for neurological disease diagnosis, there is a growing research interest towards EEG biomarkers for monitoring the progression of PD [5–7]. Pathological basal ganglia oscillations in PD are related to abnormal activity of the cortex [8], which can cause lower inter-trial adherence, higher early phase deflection, and lower connectivity between right and left M1 and dorsolateral prefrontal cortex [9]. Besides, compared to healthy controls (HCs), phase-amplitude coupling of PD patients was enhanced in dorsolateral prefrontal cortex, premotor cortex, primary motor cortex and somatosensory cortex [10]. Based on these findings, deep-learning models, such as convolutional neural network (CNN) [11], convolutional recurrent neural network (CRNN) [12], and deep residual shrinkage network (TQWT–DRSN) [13] have also been successfully used to differentiate PD subjects from HCs with multi-channel resting-state EEG signals. These seminal studies indicate that EEG could potentially serve as a noninvasive diagnostic tool for PD.

Studies about EEG biomarkers monitoring the progression of PD have been popular for many years, as a non-invasive and practical tool for neurological disease diagnosis. It was found that non-linear quantifiers showed an increase in entropy and in the number of non-linear EEG segments for PDs [14]. In addition, it was also proved that PDs' EEG signals showed higher entropy with wavelet packet entropy method [5]. Five entropy measures were used to detect PD from HC, indicating that log energy entropy, threshold entropy, sure entropy, and modified-Shannon entropy were promising biomarkers for PD detection [15]. Yuvaraj et al. [16] used higher order spectra as biomarkers for PDs. Cavanagh et al. [17] proposed the obligatory neural mechanism systemic alteration which showed to be a reliable biomarker with improved performance. Jackson et al. [18] found that sharpness ratio and steepness ratio of EEG waveform shape were higher, demonstrating basal ganglia thalamocortical loops were excessively synchronized in PDs. Coelho et al. [19] proved Hjorth features could be extracted from EEG can detect PDs effectively. Anjum et al. [20] proposed an EEG-based signal processing approach to distinguish PDs and control patients. Zhang et al. [13] introduced hybrid tunable Q-factor wavelet transform and wavelet packet transform to analysis time–frequency characteristic in EEG signals of PDs, and the difference of complexity of EEG signals in patients with Parkinson and REM sleep disorders was identified. After source localization, functional-connectivity (FC) was estimated with dynamic phase-locking value method, indicating that PD patients with freezing of gait showed an impairment in executive control [21]. Conti et al. performed spectral analysis of PD EEG data in five frequency bands, and calculated FC matrices based on both coherency and imaginary part of coherency. The results showed that a significant increase in γ band power density was found in PD patients, and that reduced FC in α–β frequency bands was observed in PD patients [22]. In early onset PD patients, β band power of O1, O2, T5, T6, P3, P4, and C3 subregions significantly decreased, and interhemispheric β band coherences between the midtemporal and frontal regions was significantly increased [23]. These pioneering studies indicate that we may find signs for PD progression directly from scarp EEG signals, without source localization which is time-consuming. However, existing analytical methods generally ignore the dynamic brain activity-correlations between each pair of EEG channels.

It was found that FC was affected early in the degenerative process [4]. There is a wide interest in identifying FC states which can reflect impaired neural activity to improve diagnosis and clinical strategies of PD. Through time-varying FC states, we can reveal co-evolutionary brain activities associated with neural diseases [24–26]. Therefore, temporal dynamics of the cortical regions have often been estimated to detect PD [27–29], aiming to provide more insight into the correlation between scalp EEG alterations and cognitive deficits caused by PD. EEG amplitude synchronization between different brain subregions has been found to become stronger as PD severity increase [30]. However, from the perspective of channelwise synchronization, transient FC states have not been explored in PD diagnosis till now. Moreover, without source localization, it is unnecessary to collect magnetic resonance images to construct head model to compute EEG inverse problems. This would save a lot of time and computing resources.

In this study, dFC was specially used to indicate that how EEG signals of different scalp channels co-fluctuate over time. We extracted channelwise dFC states directly from resting-state EEG signals to find the spatiotemporal characteristic biomarkers of neural dysfunction in PD. Channelwise dFC states were first estimated with weighted symbolic mutual information (wSMI) algorithm, and critical dFC states were then classified with *k*-means clustering. Two open-source PD EEG data sets were used to validate our method (https://doi.org/10.18112/openneuro.ds002778.v1.0.4: 32 channels, 16 health controls and 15 PD subjects. https://doi.org/10.18112/openneuro.ds003490.v1.1.0: 64 channels, 25 health controls and 25 PD subjects). Here, our contribution lies in revealing that abnormal channelwise FC

states within beta frequency band can be detected from resting-state EEG signals of patients with Parkinson's disease. This work offers a more intuitive view towards the changes of dFC states across HC, PD-on, PD-off groups, which may help early diagnoses of PD.

The Background introduces the most relevant studies. In Section of Methods, we introduce data sets used in this work and the details of the proposed method. In Result section, we present results on two data sets. Section Discussion investigates the influence of the proposed method and discusses limitations of the current study and future research directions. We conclude this letter in Section Conlcusion.

Methods

Subjects

Two resting-state EEG data sets were included in this study. The first data set (https://doi.org/10.18112/openneuro.ds002778.v1.0.4) consists of 32-channel EEG data from 15 PD patients (eight female, mean age = 63.27 ± 8.20 years, on and off dopaminergic medication), and 16 age-matched healthy controls (nine female, mean age = 63.50 ± 9.67 years). All PD patients had been diagnosed by a movement disorder specialist at scrips clinic in La Jolla, California. Participants were right-handed and provided written consent in accordance to the Institutional Review Board of the University of California, San Diego and the Declaration of Helsinki [18, 31–34]. The other data set (https://doi.org/10.18112/openneuro.ds003490.v1.1.0) includes 25 PD patients (nine female, mean age = 69.68 ± 8.73 years, on and off dopaminergic medication), and 25 age-matched healthy controls (nine female, mean age = 69.32 ± 9.58 years). PD patients came in twice separated by a week, either ON or OFF medication. Healthy controls only came in once. All demographic and clinical information are summarized in Table 1.

EEG preprocessing

EEG data were preprocessed with the open-source MATLAB toolbox of EEGLAB (https://sccn.ucsd.edu/eeglab). Data were first re-referenced to mean value of all channels. Artifacts such as eye blinks, eye movements and muscle tension, were separately removed using independent component analysis (ICA), which is the most popular method to remove artifact from EEG signals. By performing blind source separation on linear mixtures of independent source signals, ICA can effectively detect, and separate a wide variety of artifactual sources in EEG records. After denoising re-reference, and artifact-removing, five frequency bands were extracted from the preprocessed EEG signals with fourth-order Butterworth bandpass filter in ERPLAB (https://github.com/lucklab/erplab), including delta (0.5–4 Hz), theta (4–8 Hz), alpha (8–13 Hz), beta (8–30 Hz) and gamma (30–50 Hz) sub-bands.

Table 1 Demographic and clinical data of the two study groups

		Scalp channels	Number	Age	Gender
Data set 1	HC	32	16	63.50 ± 9.67	9F, 7 M
	PD-off/on	32	15	63.27 ± 8.20	8F, 7 M
Data set 2	HC	64	25	69.32 ± 9.58	9F, 16 M
	PD-off/on	64	25	69.68 ± 8.73	9F, 16 M

Weighted-symbolic mutual information (wSMI)

In this study, channelwise FC was estimated by computing wSMI index, which ignores conjunctions of identical or opposite sign symbols. This offers a new measure to quantify information sharing between two time series [35]. Actually, wSMI is a form of weighted relative entropy, and it can assess the extent to which two EEG signals exhibit non-random linear or non-linear joint-fluctuations. The evidence [36] suggests that wSMI could robustly estimate FC. The symbolic transformation depends on the number of EEG samples that are used to define the symbols and on the temporal separation between EEG signals. Here, we use it to evaluate the extent to which two channels of EEG signals present non-random joint fluctuations. As mentioned in [37], this method presents threefold advantages. First, it allows a fast and robust entropy estimation of EEG signals, as the symbolic transformation depends only on the length of the symbols and their temporal separation. Second, wSMI provides an efficient way to detect nonlinear coupling, without making hypotheses about the type of interactions and. Third, wSMI weights are estimated via fully utilizing nontrivial pairs of symbols, discarding the spurious correlations between EEG signals arising from common sources.

The joint probability of each pair of symbols occurring simultaneously in two different EEG channels was computed to infer the mutual information between EEG signals. The EEG samples are first transformed into sequences of discrete symbols. We chose the kernel k to be 3, implying that the symbols are constituted of three elements, leading to six different potential symbols in total [35, 37]. wSMI index is defined as follows:

$$wSMI\left(\hat{X},\hat{Y}\right)=\frac{1}{\log\left(k!\right)}\sum_{\hat{x}\in\hat{X}}\sum_{\hat{y}\in\hat{Y}}w\left(\hat{x},\hat{y}\right)p\left(\hat{x},\hat{y}\right)\log\frac{p\left(\hat{x},\hat{y}\right)}{p\left(\hat{x}\right)p\left(\hat{y}\right)} \tag{1}$$

where log() is logarithmic function, $p()$ is probability function. wSMI looks for qualitative or "symbolic" patterns of increase or decrease in signal, which allows a robust and fast estimation of the signals' entropies. As the sliding window size within the range of 30 s to 1 min can capture reliable resting-state brain dynamics [14, 38, 39], the windows size is set to 40 s in this study (Fig. 1).

Clustering of channelwise dFC states

K-means is an unsupervised clustering algorithm that can divide dFC observations into clusters based on their mean [40, 41]. In this study, for each frequency sub-band, we employed *k*-means clustering method to partition dFC states into several clusters. This method iterates through two steps: first, it assigns each FC state to the cluster whose prototype it is most similar with. It then re-calculates cluster prototypes, which is often done by averaging over the newly assigned FC states. The algorithm continues iterating over these two steps until the change in assignments of FC state samples between iterations are low enough to reach a pre-set threshold [42]. The number of clusters was determined as $k=6$, which was within a reasonable range (4–7) consistent with previous dFC studies on different brain disorders [24].

k-means clustering algorithm used in this work was summarized as follows:

- Step 1: Preset k sample points as initial clustering centers $(\mathbf{c}_1^{(1)}, \mathbf{c}_2^{(1)}, \ldots \mathbf{c}_k^{(1)})$
- Step 2: Calculate distance metric:

$$d(\mathbf{x}, \mathbf{c}) = 1 - \frac{(\mathbf{x} - \overline{\mathbf{x}})(\mathbf{c} - \overline{\mathbf{c}})^T}{\sqrt{(\mathbf{x} - \overline{\mathbf{x}})(\mathbf{x} - \overline{\mathbf{x}})^T}\sqrt{(\mathbf{c} - \overline{\mathbf{c}})(\mathbf{c} - \overline{\mathbf{c}})^T}} \tag{2}$$

- Step 3: For each state sample $\mathbf{x}_t$, compute $\min\{d(\mathbf{x}_t, \mathbf{c}_i)\}$,, and assign $\mathbf{x}_t$ to $\mathbf{c}_i$ class.
- Step 4: Update the cluster center according to the new classified samples:

$$\mathbf{c}_i^{(j+1)} = \frac{1}{n_t}\sum_{t=1}^{n_i} \mathbf{x}_t \tag{3}$$

- Step 4: Update the cluster center according to the new classified samples:
- Step 5: Repeat step2–4, until $\left|\mathbf{c}_i^{(j+1)} - \mathbf{c}_i^{(j)}\right| < \sigma$. After *k*-means clustering was complete, the proportion f of individual dFC state was computed as follows:

$$f = \frac{N_{\text{state}}}{N_{\text{total}}} \tag{4}$$

where N_{state} denotes number of classified individual dFC states, and N_{total} is total number of states.

Statistical analysis

ANOVA tests across HC, PD-off, and PD-on groups were performed on the proportions of critical dFC states. We compared each state in the five frequency bands (delta, theta, alpha, beta, and gamma) by two-factor ANOVA tests. P -value ≤ 0.05 indicates statistical significance. The statistical analyses were performed using MATLAB 2021a.

Results

32-Channel resting-state EEG (Data Set1)

Here, we used elbow method to determine the optimal value for *k*-means clustering, as shown in Fig. 2. From this curve, we can find that it is appropriate to set the classifying number to 6.

Figure 3 displays the *k*-clustering results for Data Set 1 (32-channel EEG data), with the number of dFC states as 6. From top to bottom, each row represents the critical channelwise dFC states within delta (0.5–4 Hz), theta (4–8 Hz), alpha (8–13 Hz), beta (13–30 Hz) and gamma (30–50 Hz) frequency bands, respectively. Significant differences were found in proportion of state1 within beta band, and state5 and state6 in gamma band (Fig. 4), between HC and PD-off groups. For all five frequency bands, no significant differences were found between PD-off and PD-on groups. No significant difference in proportions of dFC states between HC and PD-on was identified. The proportion of each dFC state is reported in Table 2.

64-Channel resting-state EEG (Data Set2)

For the second EEG data set, elbow method was also used to determine the optimal value for k-means clustering. The results are demonstrated in Fig. 5. We found that it is also appropriate to set the classifying number to 6 for this 64-channel EEG data set.

Figure 6 displays the clustering results of Data Set 2 (64-channel EEG data), also with the number of dFC states as 6. From top to bottom, each row shows the channelwise dFC states for delta (0.5–4 Hz), theta (4–8 Hz), alpha (8–13 Hz), beta (13–30 Hz) and gamma (30–50 Hz) bands, respectively. Significant differences were found in proportions of three states (state3, state4, and state5) within delta (0.5–4 Hz) band, two states (state2 and state5) within theta (4–8 Hz) band, three states (state3, state4, and state6) within beta (13–30 Hz) band, between HC and PD-on/off groups (Fig. 7). For all frequency bands, no significant differences were found between PD-off and PD-on groups. The proportion of each state is reported in Table 3.

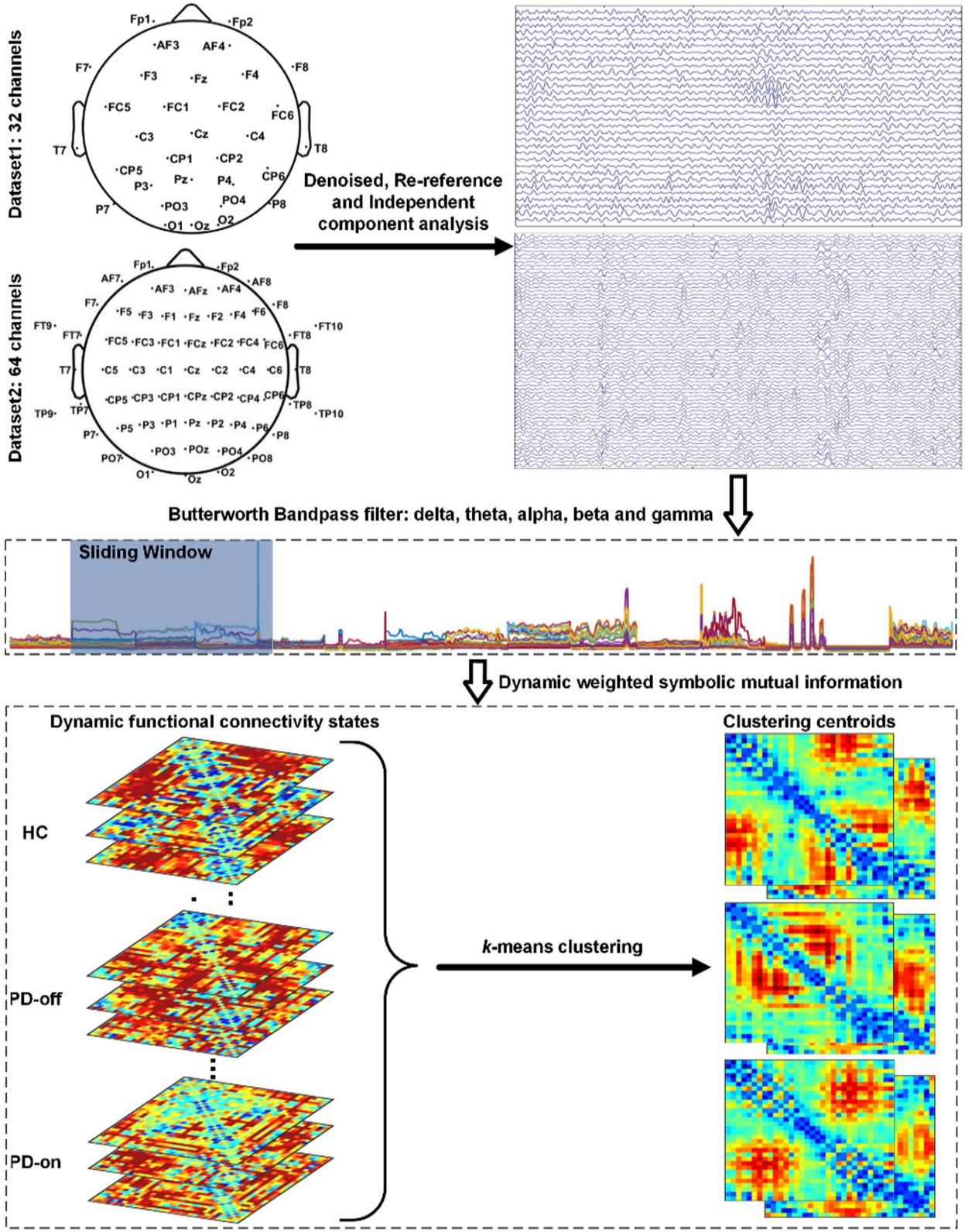

Fig. 1 Flowchart of clustering dFC states extracted from resting-state EEG signals of patients with PD. After resting-state EEG signals were preprocessed, including denoising, linearly detrended, and artifact removal, they were bandpass filtered into delta (0.5–4 Hz), theta (4–8 Hz), alpha (8–13 Hz), beta (13–30 Hz) and gamma (30–50 Hz) frequency bands. Shared information between each pair of channels was measured with wSMI algorithm. At last, centroid dFC states were determined with k-means clustering

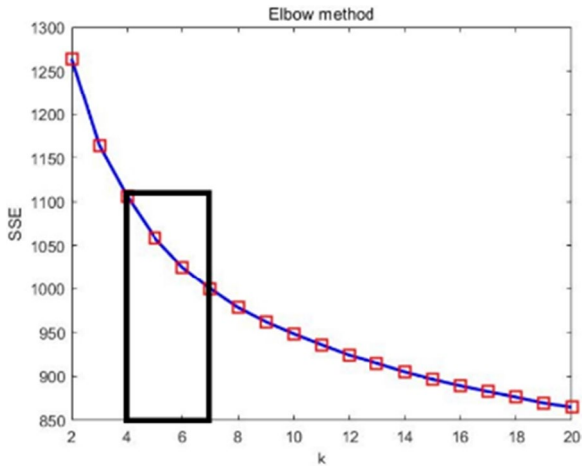

Fig. 2 Elbow method was used to find optimal value of *k*-means clustering for 32-channel resting-state EEG data set

Specifically, for Theta State 5, Beta States 4 and 6, significant differences were found only between HC and PD-on groups. We will further explore why this phenomenon exist. Of note, the classified critical states of the two data sets were not the same, and there were no direct relationships between them.

Clustering performance is based on cluster selection [40, 41]. Performance degradation may occur if a large number of clusters are selected. Selecting fewer clusters may not result in better separation. Therefore, we also investigated the influence of k on dFC state clustering. When dFC states were partitioned into four classes ($k=4$), it was found that, for the both data sets, no significant changes were found in proportions of dFC states within Beta (13–30 Hz) band. This may be due to the fact that critical centroids were not discovered when k is too small. When $k=5$, we can significantly differentiate HC and PD groups in data set 2 according to proportion of state1, state3, and state4 within Beta band. However, no significantly different dFC states within Beta band were found for data set 1. When $k=7$, no significant changes were found in the proportion of any states between HC and PD groups of data set 1. However, the proportions of state2 and state3 within Beta band was significantly different between HC and PD groups of data set 2. We also found that state4 and state7 within Gamma band were significantly differentiate HC and PD groups in Data Set 1. Taken together, in consideration of robustness, $k=6$ is most appropriate for clustering of channelwise dFC states, from resting-state EEG signals.

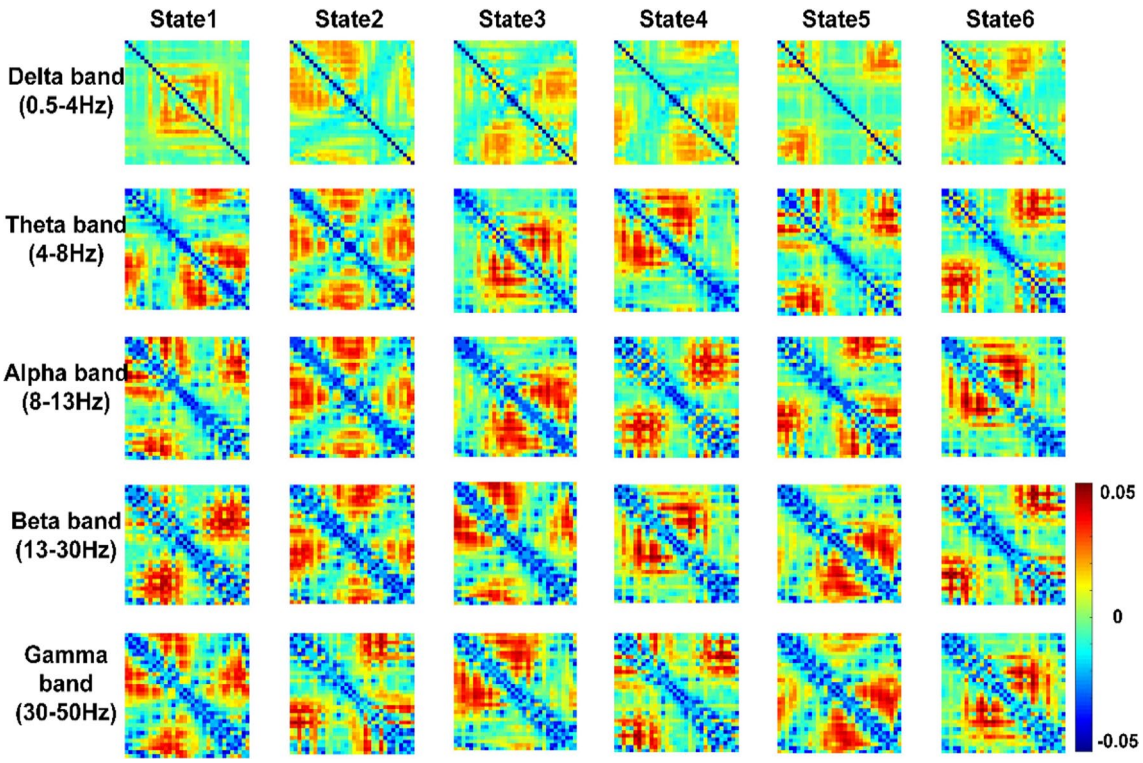

Fig. 3 Classified dFC states of 32-channel resting-state EEG data set. Six dFC states are identified. From top to bottom, each row represents the clustered dFC states for delta (0.5–4 Hz), theta (4–8 Hz), alpha (8–13 Hz), beta (13–30 Hz) and gamma (30–50 Hz) bands

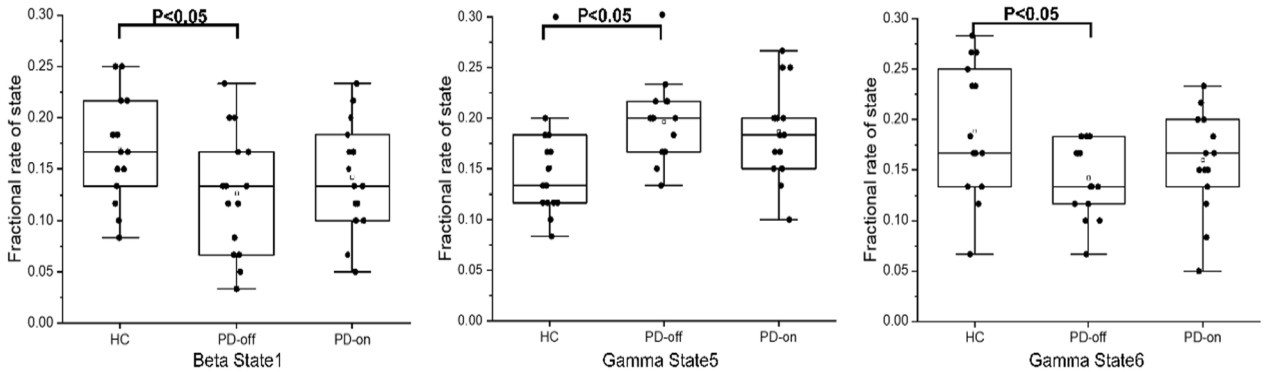

Fig. 4 ANOVA tests were performed on proportion of each dFC state. Significant differences were only found for Beta (13–30 Hz) state1, Gamma (30–50 Hz) state5 and state6 across HC, PD-off, and PD-on groups

Table 2 Proportions of dFC states of 32-channel EEG data set. (Mean ± SD)

Groups	Sub-bands	State1	State2	State3	State4	State5	State6
HC	Delta	0.170 ± 0.060	0.154 ± 0.068	0.171 ± 0.043	0.163 ± 0.053	0.169 ± 0.050	0.172 ± 0.053
	Theta	0.158 ± 0.038	0.198 ± 0.060	0.161 ± 0.051	0.169 ± 0.061	0.149 ± 0.043	0.166 ± 0.043
	Alpha	0.169 ± 0.045	0.189 ± 0.052	0.168 ± 0.048	0.160 ± 0.033	0.170 ± 0.044	0.144 ± 0.049
	Beta	0.170 ± 0.050	0.172 ± 0.072	0.169 ± 0.063	0.171 ± 0.057	0.179 ± 0.050	0.139 ± 0.045
	Gamma	0.170 ± 0.060	0.163 ± 0.077	0.181 ± 0.072	0.146 ± 0.047	0.151 ± 0.053	0.189 ± 0.064
PD-off	Delta	0.176 ± 0.052	0.143 ± 0.050	0.163 ± 0.044	0.173 ± 0.075	0.190 ± 0.042	0.154 ± 0.047
	Theta	0.169 ± 0.077	0.178 ± 0.058	0.189 ± 0.056	0.153 ± 0.043	0.159 ± 0.035	0.152 ± 0.062
	Alpha	0.171 ± 0.048	0.162 ± 0.043	0.177 ± 0.038	0.146 ± 0.050	0.186 ± 0.055	0.159 ± 0.056
	Beta	0.127 ± 0.059	0.196 ± 0.056	0.189 ± 0.047	0.160 ± 0.050	0.181 ± 0.061	0.148 ± 0.060
	Gamma	0.177 ± 0.049	0.147 ± 0.049	0.179 ± 0.032	0.159 ± 0.043	0.197 ± 0.040	0.142 ± 0.037
PD-on	Delta	0.167 ± 0.062	0.162 ± 0.058	0.154 ± 0.048	0.196 ± 0.030	0.170 ± 0.051	0.151 ± 0.044
	Theta	0.184 ± 0.050	0.176 ± 0.053	0.163 ± 0.044	0.146 ± 0.026	0.163 ± 0.051	0.168 ± 0.052
	Alpha	0.153 ± 0.052	0.176 ± 0.048	0.171 ± 0.039	0.164 ± 0.035	0.191 ± 0.043	0.144 ± 0.052
	Beta	0.142 ± 0.053	0.163 ± 0.060	0.161 ± 0.046	0.182 ± 0.064	0.186 ± 0.036	0.166 ± 0.049
	Gamma	0.182 ± 0.034	0.167 ± 0.049	0.157 ± 0.034	0.148 ± 0.046	0.187 ± 0.046	0.160 ± 0.050

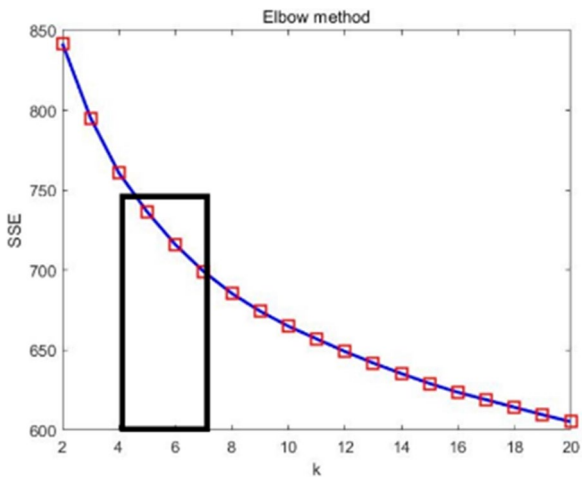

Fig. 5 Elbow method was used to find optimal value of *k*-means clustering for 64-channel resting-state EEG data set

Discussion

As damaging effects of basal ganglia dysfunction pass across the cortex [8], understanding the changes in channelwise cortical synchronization in PD is important. Using wSMI and *k*-means clustering techniques, the present study has comprehensively characterized channelwise dFC states directly extracted from scalp resting-state EEG recordings of PD patients, providing novel insights into abnormal brain synchronization related to PD. The findings indicate that the dFC states, to some extent, can differentiate PD subjects from healthy controls. Since the two open PD data sets are lack of detailed therapy information, it is difficult to assess effects of medication therapy on dFC states.

Brain network oscillations are crucial to achieve cognitive functions, which are often disrupted by PD. Although it was reported that non-motor symptoms may be related

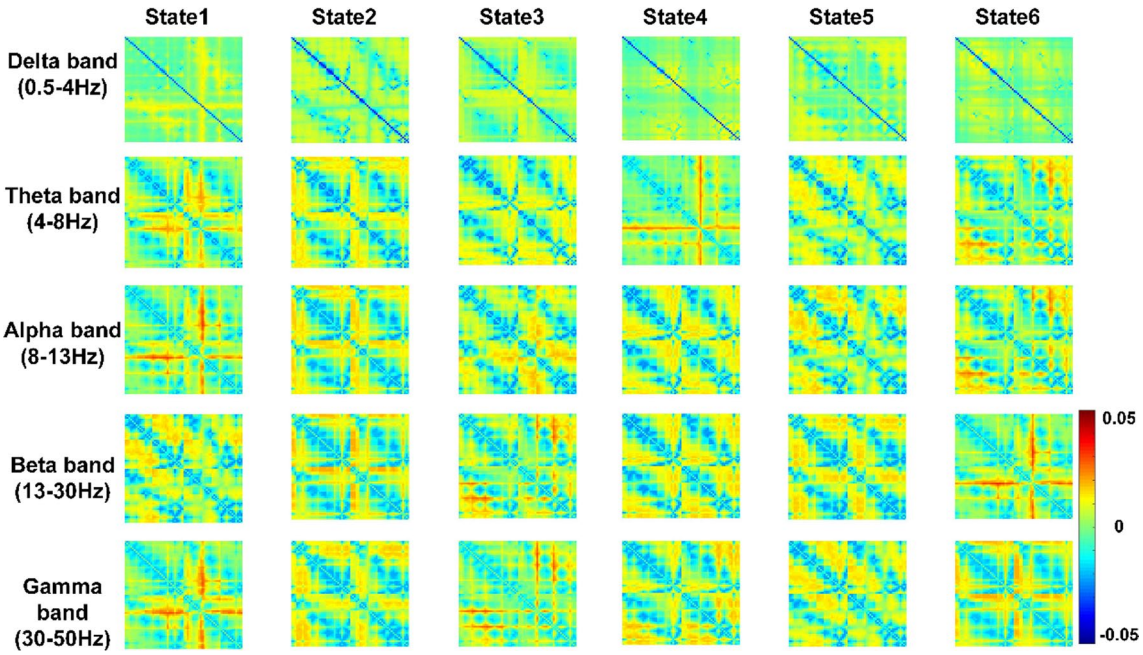

Fig. 6 Classified dFC states of 64-channel resting-state EEG data set. Six dFC states are identified. From top to bottom, each row represents the clustered dFC states for delta (0.5–4 Hz), theta (4–8 Hz), alpha (8–13 Hz), beta (13–30 Hz) and gamma (30–50 Hz) bands

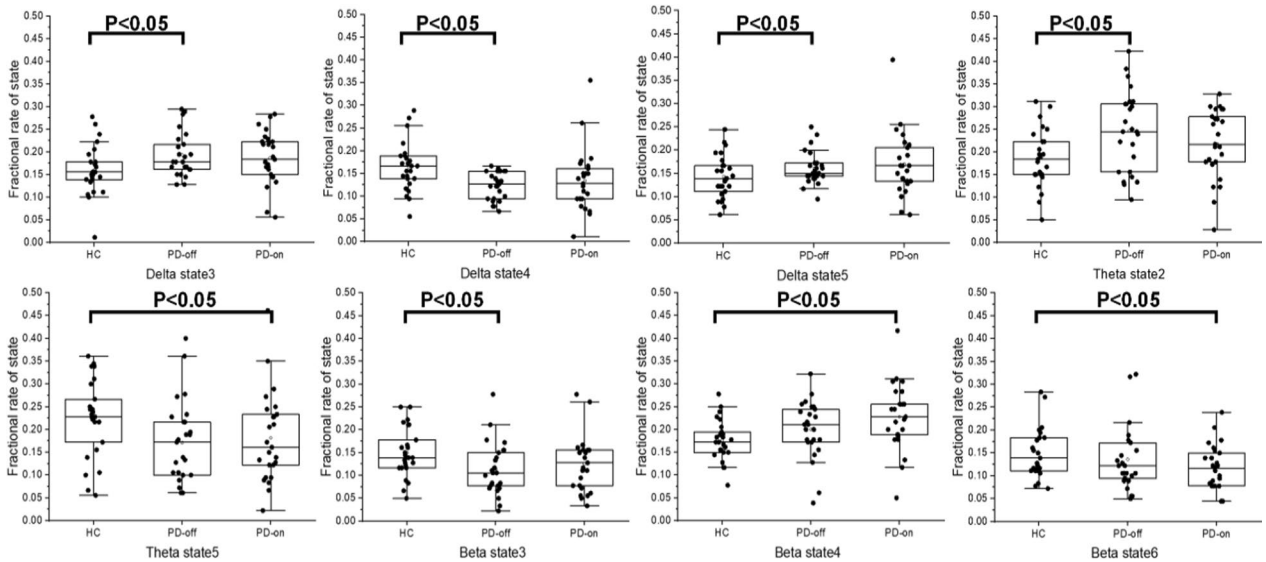

Fig. 7 ANOVA tests were performed on proportion of each dFC state. Significant differences were found for delta (0.5–4 Hz) state3, state4, state5, theta (4–8 Hz) state2, state5, and beta (13–30 Hz) state3, state4, state6 across HC, PD-off, and PD-on groups

mainly to changes in the alpha frequency band [43, 44], no significantly different FC states within alpha band were found from both data set 1 and data set 2. Otherwise, impaired channelwise dFC states (significant differences in the proportions of state5 and state6) in gamma band in PD were found for data set 1, in accordance with [12, 45]. However, no states in gamma band were found for data set 2. This may be attributed to two factors. One is distribution of scalp EEG electrodes, and the other is that the number of EEG channels is different. Many researchers consistently found that PD has been associated with increased Beta (13–30 Hz) synchronization and Beta bursts in the basal ganglia [10, 18, 46]. Compared to HCs, PD patients show a decrease in Beta frequency [47,

Table 3 Proportions of dFC states of 64-channel EEG data set. (Mean ± SD)

Groups	Sub-bands	State1	State2	State3	State4	State5	State6
HC	Delta	0.177 ± 0.047	0.201 ± 0.060	0.160 ± 0.056	0.165 ± 0.054	0.143 ± 0.047	0.154 ± 0.052
	Theta	0.149 ± 0.050	0.186 ± 0.064	0.174 ± 0.063	0.138 ± 0.049	0.224 ± 0.085	0.128 ± 0.050
	Alpha	0.148 ± 0.059	0.181 ± 0.100	0.165 ± 0.058	0.161 ± 0.045	0.202 ± 0.082	0.142 ± 0.038
	Beta	0.156 ± 0.079	0.183 ± 0.083	0.150 ± 0.054	0.176 ± 0.045	0.185 ± 0.068	0.150 ± 0.054
	Gamma	0.165 ± 0.053	0.168 ± 0.084	0.132 ± 0.064	0.178 ± 0.072	0.151 ± 0.096	0.205 ± 0.120
PD-off	Delta	0.171 ± 0.037	0.225 ± 0.049	0.193 ± 0.048	0.123 ± 0.030	0.161 ± 0.035	0.127 ± 0.038
	Theta	0.166 ± 0.045	0.246 ± 0.089	0.174 ± 0.059	0.114 ± 0.050	0.171 ± 0.091	0.128 ± 0.038
	Alpha	0.126 ± 0.066	0.222 ± 0.098	0.140 ± 0.057	0.193 ± 0.066	0.167 ± 0.073	0.152 ± 0.059
	Beta	0.152 ± 0.080	0.180 ± 0.072	0.114 ± 0.057	0.200 ± 0.064	0.218 ± 0.081	0.136 ± 0.070
	Gamma	0.155 ± 0.070	0.197 ± 0.102	0.096 ± 0.063	0.174 ± 0.065	0.176 ± 0.090	0.201 ± 0.091
PD-on	Delta	0.161 ± 0.044	0.227 ± 0.077	0.186 ± 0.058	0.134 ± 0.069	0.169 ± 0.069	0.123 ± 0.044
	Theta	0.150 ± 0.045	0.218 ± 0.077	0.186 ± 0.058	0.125 ± 0.083	0.182 ± 0.098	0.138 ± 0.067
	Alpha	0.111 ± 0.040	0.211 ± 0.096	0.145 ± 0.075	0.198 ± 0.068	0.179 ± 0.086	0.156 ± 0.066
	Beta	0.160 ± 0.115	0.175 ± 0.074	0.126 ± 0.061	0.228 ± 0.073	0.192 ± 0.090	0.119 ± 0.048
	Gamma	0.144 ± 0.048	0.186 ± 0.083	0.109 ± 0.059	0.196 ± 0.065	0.209 ± 0.120	0.156 ± 0.071

48]. Neural activity in beta frequency band was found to be excessively synchronized in PD [35]. In line with these studies, significant changes in proportions of FC states within Beta frequency band were consistently observed from both EEG data sets.

As for EEG data set 1 (32-channel), significant differences were only found in proportions of one dFC state (State1) in Beta band, and two dFC states (State5 and State6) in Gamma band. Regarding EEG data set 2 (64-channel), however, significant differences were found in proportions of more dFC states, including two dFC states (state3, state4, and state5) in Delta band, two dFC states (state2 and state5) in Theta band, and three states (state3, state4, and state6) in Beta band. This indicates that more densely distributed scalp electrodes can capture more distinguishing dFC features associated with PD from resting-state EEG signals. The reason might be that higher-density EEG electrodes can provide higher spatial-resolution physiological information over time about PDs.

While there has been debates on PD prediction from scalp EEG, there is a strong consensus that dFC patterns in EEG signals and their mutual transformation have a neuronal activity origin. And this may offer a new understanding of PD-related brain changes. Here, through analyzing changing patterns of the clustered dFC states from resting-state scalp EEG signals, our work may help find a convenient and low-cost biomarker for PD in early stage, and reflect co-fluctuating patterns between each pair of EEG channels over time during PD progression. Successful performance of cognitive tasks requires precise synchronization between brain subregions. High temporal resolution of EEG signals allows the study of transient functional connectivity between different brain subregions. In next step, we will recruit more PD patients with motor and non-motor symptoms to explore dFC specifically associated with distinct PD symptoms.

Although wSMI provides an efficient way to detect nonlinear coupling and makes few hypotheses on the type of interactions of EEG signals, it may have low sensitivity when considering larger frequency range. In addition, the number of test subjects is relatively small. In future, more PD subjects would be recruited to evaluate our methods.

Conclusions

Using wSMI and *k*-means clustering algorithms, this study revealed critical channelwise dFC states related to PD. Significant changes in proportion of dFC states within beta frequency band were consistently observed in these both data sets. These findings lay a foundation for understanding how channelwise dFC states related to PD. Such objective and convenient scalp–EEG metric for PD would have some indications for early diagnosis of PD. In future work, we will further assess the effectiveness of other algorithms (such as fuzzy *c*-means and hybrid PSO *k*-means) in classifying channelwise dFC states.

Abbreviations

PD	Parkinson's disease
EEG	Electroencephalogram
dFC	Dynamic functional-connectivity
wSMI	Weighted-symbolic mutual information
AD	Alzheimer's disease
CNN	Convolution neural network
CRNN	Convolution recurrent neural network
HC	Healthy control
PD-off	Parkinson patients without medicine
PD-on	Parkinson patients on medicine
ICA	Independent component analysis

Acknowledgements
Not applicable.

Author contributions
H Ding and X Weng analyzed the data, plotted the graphs, and explained the results. M Xu helped to preprocess EEG signals. J Shen and Z Wu improved English expressions. All authors read and approved the final manuscript. Z Wu supervised this work.

Funding
The research was supported by Natural Science Foundation of Zhejiang Province (LY20E070005).

Availability of data and materials
Data and materials are available from the corresponding author on reasonable request.

Declarations

Ethics approval and consent to participate
Not applicable.

Consent for publication
All authors have approved the manuscript and agreed with its submission to The Egyptian Journal of Neurology, Psychiatry and Neurosurgery.

Competing interests
The authors declare that they have no conflict of interest.

Received: 27 October 2023 Accepted: 6 May 2024
Published online: 21 May 2024

References

1. Sveinbjornsdottir S. The clinical symptoms of Parkinson's disease. J Neurochem. 2016;139:318–24. https://doi.org/10.1111/jnc.13691.
2. Saeed U, Compagnone J, Aviv R, Strafella A, Black S, Lang A, Masellis M. Imaging biomarkers in Parkinson's disease and Parkinsonian syndromes: current and emerging concepts. Transl Neurodegen. 2017. https://doi.org/10.1186/s40035-017-0076-6.
3. Hassin-Baer S, Cohen O, Israeli-Korn S, Yahalom G, Benizri S, Sand D, Issachar G, Geva A, Shani-Hershkovich R, Peremen Z. Identification of an early-stage Parkinson's disease neuromarker using event-related potentials, brain network analytics and machine-learning. PLoS ONE. 2022;17(1): e0261947. https://doi.org/10.1371/journal.pone.0261947.
4. Droby A, Nosatzki S, Edry Y, Thaler A, Giladi N, Mirelman A, Maidan I. The interplay between structural and functional connectivity in early stage Parkinson's disease patients. J Neurol Sci. 2022;442: 120452. https://doi.org/10.1016/j.jns.2022.120452.
5. Han C, Wang J, Yi G, Che Y. Investigation of EEG abnormalities in the early stage of Parkinson's disease. Cogn Neurodyn. 2013;7(4):351–9. https://doi.org/10.1007/s11571-013-9247-z.
6. Klassen B, Hentz J, Shill H, Driver-Dunckley E, Evidente V, Sabbagh N, Adler C, Caviness J. Quantitative EEG as a predictive biomarker for Parkinson disease dementia. Neurology. 2011;77(2):118–24. https://doi.org/10.1212/wnl.0b013e318224af8d.
7. Geraedts V, Boon L, Marinus J, Gouw A, van Hilten J, Stam C, Tannemaat M, Contarino M. Clinical correlates of quantitative EEG in Parkinson disease. Neurology. 2018. https://doi.org/10.1212/WNL.0000000000006473.
8. Palmer S, Wen-Hsin Lee P, Wang Z, Au W, McKeown M. θ, β But not α-band EEG connectivity has implications for dual task performance in Parkinson's disease. Parkinsonism Relat Disord. 2010;16(6):393–7. https://doi.org/10.1016/j.parkreldis.2010.03.001.
9. Maidan I, Zifman N, Hausdorff J, Giladi N, Levy-Lamdan O, Mirelman A. A multimodal approach using TMS and EEG reveals neurophysiological changes in Parkinson's disease. Parkinsonism Relat Disord. 2021;89:28–33. https://doi.org/10.1016/j.parkreldis.2021.06.018.
10. Gong R, Wegscheider M, Mühlberg C, Gast R, Fricke C, Rumpf J, Nikulin V, Knosche T, Classen J. Spatiotemporal features of β-γ phase-amplitude coupling in Parkinson's disease derived from scalp EEG. Brain. 2020. https://doi.org/10.1093/brain/awaa400.
11. Oh S, Hagiwara Y, Raghavendra U, Yuvaraj R, Arunkumar N, Murugappan M, Acharya U. A deep learning approach for Parkinson's disease diagnosis from EEG signals. Neural Comput Appl. 2018. https://doi.org/10.1007/s00521-018-3689-5.
12. Lee S, Hussein R, Ward R, Jane Wang Z, McKeown M. A convolutional-recurrent neural network approach to resting-state EEG classification in Parkinson's disease. J Neurosci Methods. 2021;361: 109282. https://doi.org/10.1016/j.jneumeth.2021.109282.
13. Zhang R, Jia J, Zhang R. EEG analysis of Parkinson's disease using time–frequency analysis and deep learning. Biomed Signal Process Control. 2022;78: 103883. https://doi.org/10.1016/j.bspc.2022.103883.
14. Pezard L, Jech R, Růžička E. Investigation of non-linear properties of multichannel EEG in the early stages of Parkinson's disease. Clin Neurophysiol. 2001;112(1):38–45. https://doi.org/10.1016/s1388-2457(00)00512-5.
15. Aljalal M, Aldosari S, Molinas M, AlSharabi K, Alturki F. Detection of Parkinson's disease from EEG signals using discrete wavelet transform, different entropy measures, and machine learning techniques. Sci Rep. 2022;12:22547. https://doi.org/10.1038/s41598-022-26644-7.
16. Yuvaraj R, Rajendra Acharya U, Hagiwara Y. A novel Parkinson's Disease Diagnosis Index using higher-order spectra features in EEG signals. Neural Comput Appl. 2016;30(4):1225–35. https://doi.org/10.1007/s00521-016-2756-z.
17. Cavanagh J, Kumar P, Mueller A, Richardson S, Mueen A. Diminished EEG habituation to novel events effectively classifies Parkinson's patients. Clin Neurophysiol. 2018;129(2):409–18. https://doi.org/10.1016/j.clinph.2017.11.023.
18. Jackson N, Cole S, Voytek B, Swann N. Characteristics of waveform shape in Parkinson's disease detected with scalp electroencephalography. Eneuro. 2019. https://doi.org/10.1523/eneuro.0151-19.2019.
19. Coelho B, Massaranduba A, Souza C, Viana G, Brys I, Ramos R. Parkinson's disease effective biomarkers based on Hjorth features improved by machine learning. Expert Syst Appl. 2023. https://doi.org/10.1016/j.eswa.2022.118772.
20. Anjum M, Dasgupta S, Mudumbai R, Singh A, Cavanagh J, Narayanan N. Linear predictive coding distinguishes spectral EEG features of Parkinson's disease. Parkinsonism Relat Disord. 2020. https://doi.org/10.1016/j.parkreldis.2020.08.001.
21. Gerard M, Bayot M, Derambure P, Dujardin K, Defebvre L, Betrouni N, Delval A. EEG-based functional connectivity and executive control in patients with Parkinson's disease and freezing of gait. Clin Neurophysiol. 2022;137:207–15. https://doi.org/10.1016/j.clinph.2022.01.128.
22. Conti M, Bovenzi R, Garasto E, Schirinzi T, Placidi F, Mercuri N, Cerroni R, Pierantozzi M, Stefani A. Brain functional connectivity in de novo Parkinson's disease patients based on clinical EEG. Front Neurol. 2022;13:844745. https://doi.org/10.3389/fneur.2022.844745.
23. He X, Zhang Y, Chen J, Xie C, Gan R, Yang R, Wang L, Nie K, Wang L. The patterns of EEG changes in early-onset Parkinson's disease patients. Int J Neurosci. 2017;127(11):1028–35. https://doi.org/10.1080/00207454.2017.1304393.
24. Fu Z, Iraji A, Turner J, Sui J, Miller R, Pearlson G, Calhoun V. Dynamic state with covarying brain activity-connectivity: on the pathophysiology of schizophrenia. Neuroimage. 2021;224:117385. https://doi.org/10.1016/j.neuroimage.2020.117385.
25. Iyer K, Au T, Angwin A, Copland D, Dissanayaka N. Theta and gamma connectivity is linked with affective and cognitive symptoms in Parkinson's disease. J Affect Disord. 2020. https://doi.org/10.1016/j.jad.2020.08.086.
26. Michel C, Koenig T. EEG microstates as a tool for studying the temporal dynamics of whole-brain neuronal networks: a review. Neuroimage. 2017. https://doi.org/10.1016/j.neuroimage.2017.11.062.
27. Betrouni N, Alazard E, Bayot M, Carey G, Derambure P, Defebvre L, Leentjens A, Delval A, Dujardin K. Anxiety in Parkinson's disease: a resting-state high density EEG study. Neurophysiol Clin. 2016;7661(3):183–264. https://doi.org/10.1016/j.neucli.2022.01.001.
28. Oswal A, Brown P, Litvak V. Movement related dynamics of subthalmocortical alpha connectivity in Parkinson's disease. Neuroimage. 2013;70:132–42. https://doi.org/10.1016/j.neuroimage.2012.12.041.

29. Stoffers D, Bosboom J, Deijen J, Wolters E, Stam C, Berendse H. Increased cortico-cortical functional connectivity in early-stage Parkinson's disease: an MEG study. Neuroimage. 2008;41(2):212–22. https://doi.org/10.1016/j.neuroimage.2008.02.027.
30. Asher E, Plotnik M, Günther M, Moshel S, Levy O, Havlin S, Kantelhardt J, Bartsch R. Connectivity of EEG synchronization networks increases for Parkinson's disease patients with freezing of gait. Commun Biol. 2021. https://doi.org/10.1038/s42003-021-02544-w.
31. Swann N, de Hemptinne C, Aron A, Ostrem J, Knight R, Starr P. Elevated synchrony in Parkinson disease detected with electroencephalography. Ann Neurol. 2015;78(5):742–50. https://doi.org/10.1002/ana.24507.
32. George J, Strunk J, Mak-McCully R, Houser M, Poizner H, Aron A. Dopaminergic therapy in Parkinson's disease decreases cortical beta band coherence in the resting state and increases cortical beta band power during executive control. NeuroImage Clin. 2013;3:261–70. https://doi.org/10.1016/j.nicl.2013.07.013.
33. Pernet C, Appelhoff S, Gorgolewski K, Flandin G, Phillips C, Delorme A, Oostenveld R. EEG-BIDS, an extension to the brain imaging data structure for electroencephalography. Sci Data. 2019. https://doi.org/10.1038/s41597-019-0104-8.
34. Appelhoff S, Sanderson M, Brooks T, Vliet M, Quentin R, Holdgraf C, Chaumon M, Mikulan E, Tavabi K, Höchenberger R, Welke D, Brunner C, Rockhill A, Larson E, Gramfort A, Jas M. MNE-BIDS: organizing electrophysiological data into the BIDS format and facilitating their analysis. J Open Source Softw. 2019;44:1896. https://doi.org/10.21105/joss.01896.
35. Imperatori L, Betta M, Cecchetti L, Canales-Johnson A, Ricciardi E, Siclari F, Pietrini P, Chennu S, Bernardi G. EEG functional connectivity metrics wPLI and wSMI account for distinct types of brain functional interactions. Sci Rep. 2019. https://doi.org/10.1038/s41598-019-45289-7.
36. Bourdillon P, Hermann B, Guénot M, Bastuji H, Isnard J, King J, Sitt J, Naccache L. Brain-scale cortico-cortical functional connectivity in the delta-theta band is a robust signature of conscious states: an intracranial and scalp EEG study. Sci Rep. 2020;10:14037. https://doi.org/10.1038/s41598-020-70447-7.
37. King J, Sitt J, Faugeras F, Rohaut B, El Karoui I, Cohen L, Naccache L, Dehaene S. Information sharing in the brain indexes consciousness in noncommunicative patients. Curr Biol. 2013;23(19):1914–9. https://doi.org/10.1016/j.cub.2013.07.075.
38. Fu Z, Tu Y, Di X, Du Y, Pearlson G, Turner J, Biswal B, Zhang Z, Calhoun V. Characterizing dynamic amplitude of low-frequency fluctuation and its relationship with dynamic functional connectivity: an application to schizophrenia. Neuroimage. 2017. https://doi.org/10.1016/j.neuroimage.2017.09.035.
39. Díez-Cirarda M, Strafella A, Kim J, Peña J, Ojeda N, Cabrera-Zubizarreta A, Ibarretxe-Bilbao N. Dynamic functional connectivity in Parkinson's disease patients with mild cognitive impairment and normal cognition. NeuroImage Clin. 2018;17:847–55. https://doi.org/10.1016/j.nicl.2017.12.013.
40. Bablani A, Edla D, Kuppili V, Ramesh D. A multi stage EEG data classification using k-means and feed forward neural network. Clin Epidemiol Glob Health. 2020;8:718–24. https://doi.org/10.1016/j.cegh.2020.01.008.
41. Orhan U, Hekim M, Ozer M. EEG signals classification using the K-means clustering and a multilayer perceptron neural network model. Expert Syst Appl. 2011;38:13475–81. https://doi.org/10.1016/j.eswa.2011.04.149.
42. Khan S, Ahmad A. Cluster center initialization algorithm for K-modes clustering. Expert Syst Appl. 2013;40(18):7444–56. https://doi.org/10.1016/j.eswa.2013.07.002.
43. Bočková M, Rektor I. Impairment of brain functions in Parkinson's disease reflected by alterations in neural connectivity in EEG studies: a viewpoint. Clin Neurophysiol. 2019;130(2):239–47. https://doi.org/10.1016/j.clinph.2018.11.013.
44. Mano T, Kinugawa K, Ozaki M, Kataoka H, Sugie K. Neural synchronization analysis of electroencephalography coherence in patients with Parkinson's disease-related mild cognitive impairment. Clini Parkinsonism Related Disord. 2022;6: 100140. https://doi.org/10.1016/j.prdoa.2022.100140.
45. Muthuraman M, Bange M, Koirala N, Ciolac D, Pintea B, Glaser M, Tinkhauser G, Brown P, Deuschl G, Groppa S. Cross-frequency coupling between gamma oscillations and deep brain stimulation frequency in Parkinson's disease. Brain. 2020. https://doi.org/10.1093/brain/awaa297.
46. Kehnemouyi Y, Wilkins K, Anidi C, Anderson R, Afzal M, Bronte-Stewart H. Modulation of beta bursts in subthalamic sensorimotor circuits predicts improvement in bradykinesia. Brain. 2020. https://doi.org/10.1093/brain/awaa394.
47. Soikkeli R, Partanen J, Soininen H, Pääkkönen A, Riekkinen P. Slowing of EEG in Parkinson's disease. Electroencephalogr Clin Neurophysiol. 1991;79(3):159–65. https://doi.org/10.1016/0013-4694(91)90134-p.
48. Stoffers D, Bosboom J, Deijen J, Wolters E, Berendse H, Stam C. Slowing of oscillatory brain activity is a stable characteristic of Parkinson's disease without dementia. Brain. 2007;130(7):1847–60. https://doi.org/10.1093/brain/awm034.

Publisher's Note